

LCollision: Fast Generation of Collision-Free Human Poses using Learned Non-Penetration Constraints

Qingyang Tan¹, Zherong Pan², Dinesh Manocha¹

¹ Department of Computer Science, University of Maryland at College Park

² Department of Computer Science, University of Illinois Urbana-Champaign

qytan@umd.com, zherong@illinois.edu, dmanocha@umd.edu

Abstract

We present a learning-based method (LCollision) that synthesizes collision-free 3D human poses. At the crux of our approach is a novel deep architecture that simultaneously decodes new human poses from the latent space and classifies the collision status. These two components of our architecture are used as the objective function and surrogate hard-constraints in a constrained-optimization algorithm for collision-free human pose generation. A novel aspect of our approach is the use of a bilevel autoencoder that decomposes whole-body collisions into groups of collisions between localized body parts. We show that solving our constrained optimization formulation can resolve significantly more collision artifacts than prior learning algorithms. Furthermore, in a large test set of 2.5×10^6 randomized poses from three major datasets, our architecture achieves a collision-prediction accuracy of 94.1% with 80x speedup over exact collision detection algorithms. To the best of our knowledge, LCollision is the first approach that can obtain high accuracy in terms of handling non-penetration and collision constraints in a learning framework.

1 Introduction

There has been considerable work on developing learning algorithms on 3D objects, represented as point clouds (Qi et al. 2017), meshes (Hanocka et al. 2019), volumetric grids (Wang, Liu, and Tong 2020), and physical objects (Li et al. 2019). As these algorithms are used for different applications, a major challenge is accounting for user requirements and physics-based constraints. Modeling these constraints can significantly improve the robustness by preserving some known criteria for “correct” predictions. For example, we need to consider various forces and dynamics constraints for differential simulation (Qiao et al. 2020). Moreover, a reliable robot motion planner should preserve a clearance distance from obstacles (Pham, De Magistris, and Tachibana 2018).

In this paper, we mainly deal with the problem of the fast generation of human poses. Recently, 3D mesh representations have been used for learning-based human pose synthesis (Tretschk et al. 2020; Bouritsas et al. 2019; Ranjan et al. 2018; Bagautdinov et al. 2018; Tan et al. 2018a). These methods learn a manifold of plausible human poses from a dataset, represented as the latent space of a deep autoencoder. After training, they can generate human poses for

different applications, including interactive rigging, human pose recognition from images and videos, and VR games. However, current learning-based methods do not account for any physics-based requirements such as (self-)collision-free constraints and thereby result in penetrations or other artifacts (Tretschk et al. 2020; Bouritsas et al. 2019; Ranjan et al. 2018; Bagautdinov et al. 2018; Tan et al. 2018a). On the other hand, non-learning-based methods for character rigging (Shi et al. 2007) and physics-based simulation (Barbić and James 2010) can detect and explicitly handle the collisions using numerical methods. Our goal is to enhance learned-based methods with similar collision handling capabilities.

Although 3D data representations explicitly allow for the formulation of such constraints, satisfying these hard constraints in an end-to-end learning system has been a long-standing open problem. Prior works treat user requirements as hard constraints and enforce them in one of three ways. First, classical second-order methods (Boggs and Tolle 1995) for constrained optimization can enforce exact hard constraints on the parameters of the neural network. Second, variants of the stochastic projected gradient descend (Marquez Neila, Salzmann, and Fua 2017; Kervadec et al. 2019) have been proposed to approximately satisfy the constraints on the neural network parameters. Finally, differentiable optimization layers (Pham, De Magistris, and Tachibana 2018; Agrawal et al. 2019) can modify the neural network output to satisfy such constraints. However, these methods are either limited to convex constraints, impractical for large networks or do not provide sufficient accuracy.

Main Results: We present a new learning algorithm (LCollision) to generate human poses that satisfy collision-free hard constraints. Our approach treats the non-penetration constraints as hard constraints of an optimization solver during runtime. The feasible domain corresponding to these hard constraints is learned during the training time. The novel components of our approach include:

- **Constrained Optimization Using Neural Network Function Approximation:** Instead of using exact collision-response, learning the feasible domain using a neural network provides approximate sub-gradients via back-propagation, which is much faster than exact collision-checking algorithms.
- **Collision Decomposition:** Since a collision only affects local regions of the human body, we use an appropriate representation to capture these local effects. Each point

on the human body is softly assigned to a set of local domains, and the collision penalty loss is decomposed to these local domains, accordingly.

- **Hybrid Ranking, Potential Energy, and Entropy Loss:**

Although exact hard constraints correspond to a binary loss (violation or non-violation), this loss should be differentiable so that constrained optimizations can be guided by gradient information. We propose using a penetration depth formulation (Zhang et al. 2007) as collision metric to offer gradient direction and then use ranking loss to enforce the relative differences between each sample.

We have implemented these algorithms and evaluated the performance on the SCAPE dataset (Anguelov et al. 2005), the MIT-Swing dataset (Vlasic et al. 2008), and the MIT Jumping dataset (Vlasic et al. 2008). Combining these techniques, we achieve an accuracy of 94.1%, a false positive rate of 6.1%, and a false negative rate of 5.7% when predicting collisions for 2.5×10^6 randomized testing poses from these datasets. After learning the feasible domain, solving a constrained optimization for a collision-free human pose with 2161 vertices takes 2.095 iterations and 0.25s on average. Moreover, our learned collision detector is 80 \times faster than prior exact collision detection methods (Pan, Chitta, and Manocha 2012).

2 Related Work

We review related works on human pose estimation and synthesis, collision detection and response, and deep network training with hard constraints.

Human Pose Estimation & Synthesis: There is considerable work on human pose estimation and synthesis. Earlier methods (Leibe, Seemann, and Schiele 2005) represent a pedestrian as a bounding box. An improved algorithm was proposed in (Agarwal and Triggs 2005), and this algorithm predicts the 55-D joint angles for a skeletal human pose. More accurate prediction results have been proposed in (Rogez et al. 2008) using random forests and in (Toshev and Szegedy 2014) using convolutional neural networks. Our approach is based on recent learning methods (Tan et al. 2018a; Tretschk et al. 2020) that use 3D meshes to generate detailed human poses. Mesh-based representations are inherently difficult to learn due to the intrinsic high-dimensionality, and the resulting algorithms can produce sub-optimal results that may consist of various artifacts such as self-penetrations, noisy mesh surfaces, and flipped meshes. In view of these problems, (Villegas et al. 2018) only computes skeletal poses using learning and then uses skinning to recover the mesh-based representation. However, this approach requires additional skeleton-mesh correspondence information, which is typically unavailable in many datasets including SCAPE (Anguelov et al. 2005).

Collision Detection & Response: An important criterion of “correct” human body shapes is that they are (self-) collision-free, i.e. elements of the mesh do not penetrate each other. Collision detection and response computations have been well-studied, with many practical algorithms proposed for large-scale 3D meshes (Pan, Chitta, and Manocha 2012; Kim, Lin, and Manocha 2018) that can be used to re-

solve penetrations. Collisions can be handled in a discrete or continuous manner. Discrete collision handling (Kim, Lin, and Manocha 2018) assumes that meshes can occasionally reach an invalid status with penetrations and therefore check for collisions at fixed time intervals to resolve them. In contrast, continuous collision detection algorithms try to estimate the time instance corresponding to the first contact and use that information to maintain non-penetration configurations. These methods use a probing strategy, known as continuous collision detection (CCD) (Tang et al. 2009; Bridson, Fedkiw, and Anderson 2002), by making some assumptions about the interpolating motion between two time instances and then using analytic methods to predict the time of the collision. In theory, we can use different collision handling methods to avoid penetrations in a 3D mesh of a human pose. However, there are two practical challenges. First, collision response is a physical behavior tightly coupled with a physics-based model of the human body. However, modeling the physical deformations of a human body can be computationally expensive. The running time for simulating one timestep of a human body can be more than 20 seconds (Smith, Goes, and Kim 2018) and is too long for interactive applications. Second, many collision handling algorithms require a volumetric mesh, while many applications of human pose synthesis rely on surface meshes. Many techniques have also been proposed to estimate the extent of penetration between complex 3D geometric models, including penetration depth computation (Zhang et al. 2007; Kim et al. 2002; Burgard, Brock, and Stachniss 2008). However, these formulations can be non-smooth and expensive, and therefore cannot be directly used for optimization-based collision avoidance.

Training Deep Networks with Hard Constraints: An additional layer of challenge is to incorporate collision handling into a deep learning framework. In particular, state-of-the-art deep learning methods are unable to handle such hard constraints. Constraints on neural network parameters (Ravi et al. 2019) are used for regularizing the network training and can be approximately enforced by using variants of the projected gradient descend algorithm. On the other hand, constraints on neural network output model application-specific requirements such as collision-free constraints. Prior works (Pham, De Magistris, and Tachibana 2018; Agrawal et al. 2019; Marquez Neila, Salzmann, and Fua 2017; Nandwani et al. 2019) use a similar approach to enforce hard constraints: converting the constraint optimization into an unconstrained min-max optimization, which can be solved approximately by simultaneously updating the primal and dual variables. A special case arises when the hard constraints are convex; then the constrained optimization can be solved efficiently with exact constraint enforcement (Pham, De Magistris, and Tachibana 2018; Agrawal et al. 2019). However, the collision-free constraints in our applications are neither convex nor smooth.

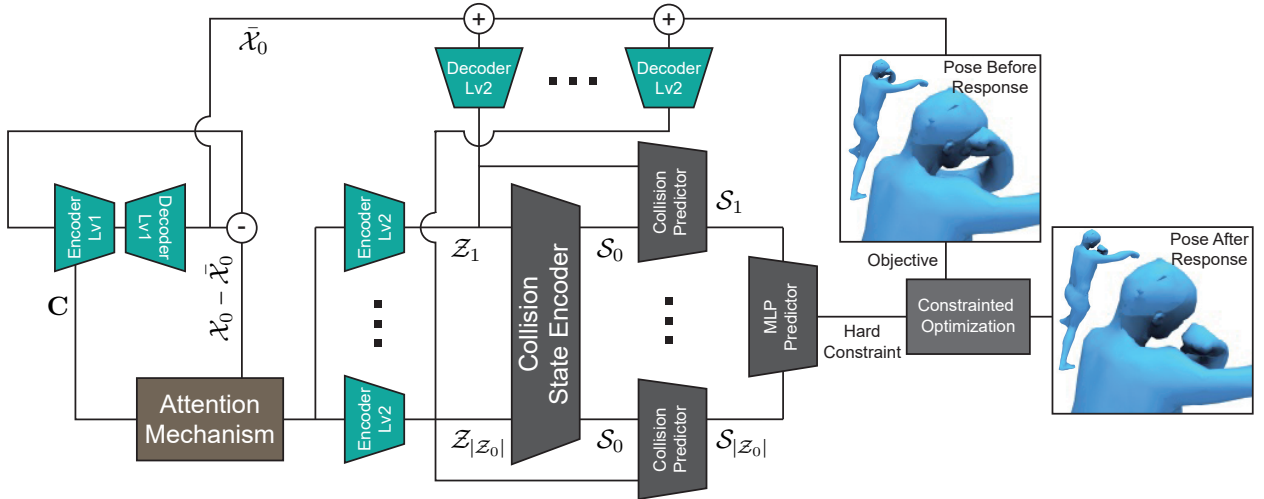


Figure 1: Our network architecture combines the domain decomposed human pose embedding framework (green) and a novel collision state estimator (gray). Given an input pose, we use a weight-shared, level-1 autoencoder to learn a global shape embedding. The error on each domain is further reduced using a set of level-2 autoencoders. Both the level-1 and level-2 autoencoders’ latent codes are used to predict a global collision state. Finally, the latent code of each level-2 autoencoder is compared against the global collision state to infer a localized penetration depth. These inferred penetrations are used as hard constraints in a constrained optimization framework for collision handling.

3 Human Pose Generation & Collision-Free Constraints

Recent methods (Tretschk et al. 2020; Bouritsas et al. 2019; Ranjan et al. 2018; Bagautdinov et al. 2018; Tan et al. 2018a) have used neural networks to generate new poses from a small set of examples. They first compute an embedding space for the dataset and then sample the new latent codes to reconstruct new human poses. In this section, we give an overview of the process of computing the embedding space for human pose generation and highlight the collision-free constraints that LCollision tries to satisfy.

3.1 Human Pose Embedding

Our method extends the algorithm in (Tan et al. 2018b), which has the ability to extract local deformation components (more details given in the appendix). We represent human models as triangle meshes – a special graph $\mathcal{G} = \langle \mathcal{V}, \mathcal{E} \rangle$, with \mathcal{V} being a set of vertices and \mathcal{E} being a set of edges. In our datasets, all the models share the same topology, i.e. \mathcal{E} is the same over all the meshes while \mathcal{V} differs. We transform \mathcal{V} to the as-consistent-as-possible (ACAP) feature space (Gao et al. 2019), denoted as $\mathcal{X} \in \mathbb{R}^{9 \times |\mathcal{V}|}$, to handle large deformations. We use a bilevel autoencoder to embed \mathcal{X} in a latent space. Both levels of the autoencoder use one graph convolutional layer and one fully connected layer. The fully-connected layer maps the feature to a K -dimensional latent code, with weights denoted as $\mathbf{C} \in \mathbb{R}^{K \times 9 \times |\mathcal{V}|}$. A sparsity loss is used to ensure that each dimension of \mathbf{C} only accounts for a group of local points.

Domain Decomposition via Attention: We use a bilevel architecture because we want the level-2 autoencoder to learn a decomposed domain of the original mesh, i.e. each level-2 autoencoder only reduces the level-1 residual on a subset of \mathcal{V} . The learned domain decomposition not only enhances the reusability and explainability of the neural net-

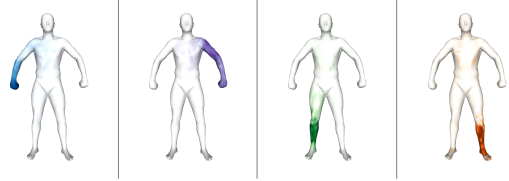


Figure 2: We show some decomposed domains on the SCAPE dataset using the learned attention mask \mathcal{M}^{ki} ; these domains are highlighted in different colors. The shade represents the extent of the soft assignment. These are used for localized collision computations.

work but is also used to model the local collisions between body sub-parts, as explained in Section 3.3.

Each autoencoder encodes some input feature \mathcal{X} to a latent code \mathcal{Z} and then reconstructs \mathcal{Z} to feature $\bar{\mathcal{X}}$. We use subscripts to denote the index of an autoencoder, e.g., \mathcal{X}_0 , \mathcal{Z}_0 , and $\bar{\mathcal{X}}_0$ are the input, latent code, and output of the level-1 autoencoder, respectively. We assume that each entry of level-1 latent code corresponds to a sub-domain of the human body on which the residual is further reduced using one level-2 autoencoder, so there are altogether $|\mathcal{Z}_0| + 1$ autoencoders. The k th level-2 autoencoder is responsible for representing a subset of residual $\mathcal{X}_0 - \bar{\mathcal{X}}_0$. To determine the subset, an attention mask is computed as: $\mathcal{M}^{ki} = \sum_{j=1}^9 \mathbf{C}^{kj} \mathbf{C}^{kjT} / \sum_{k=1}^{|\mathcal{Z}_0|} \sum_{j=1}^9 \mathbf{C}^{kj} \mathbf{C}^{kjT}$. In addition, the input to the k th level-2 autoencoder is $\mathcal{X}_k^i = \mathcal{M}^{ki}(\mathcal{X}_0^i - \bar{\mathcal{X}}_0^i)$. The soft assignment induced by the attention mask conducts the domain decomposition in our network. We show an example of some human body parts that have been decomposed using \mathcal{M}^{ki} in Figure 2.

3.2 Collision-Free Constraints

One critical constraint is that every human body pose is collision-free, i.e. boundary elements (e.g., the triangles) on

the boundaries do not penetrate each other. However, this constraint is ignored by previous neural-network-based human pose generation methods. In this paper, our goal is to eliminate (self-)collisions in newly generated human poses. We define a self-collision as an intersection between two topologically disjointed triangles, i.e. two triangles that do not share any edges. We use the following condition to indicate a collision:

$$\mathbf{t}_p \cap \mathbf{t}_q \neq \emptyset,$$

where \mathbf{t}_p and \mathbf{t}_q are two triangles. Penetration depth (PD) is a notion that measures the extent of collision constraint violations between two objects. We define the local PD for triangle pair $(\mathbf{t}_p, \mathbf{t}_q)$ as:

$$PD_{p,q} = \min\{\|\mathbf{d}\|_2 : (\mathbf{t}_p + \mathbf{d}) \cap \mathbf{t}_q = \emptyset\},$$

where $PD_{p,q}$ is the minimum distance to move \mathbf{t}_p such that \mathbf{t}_q and \mathbf{t}_p have no overlap. The collision-free constraint can be reformulated as the constraint that $PD_{p,q} = 0$ for any (p, q) pairs corresponding to disjointed triangle pairs. One way to remove collisions in the generated human meshes is by solving the following constrained optimization:

$$\begin{aligned} & \text{min } goal \\ & \text{s.t. } PD_{p,q} = 0, \quad (p, q) \text{ disjoint,} \end{aligned}$$

where *goal* is the objective (e.g., as close as possible to a user-desired pose). Prior works solve the constrained optimization by computing $PD_{p,q}$ for all (p, q) pairs and treating each colliding $(\mathbf{t}_p, \mathbf{t}_q)$ as a standalone constraint, which is expensive to compute. Instead, we use neural network to speed up the computation.

3.3 Locality of Self-collisions

Our method is inspired by the subspace self-collision culling algorithm (SSCC) (Barbić and James 2010) and the learning-based collision simplification algorithm (Teng, Otaduy, and Kim 2014). In SSCC, the authors observe that collisions usually occur between pairs of triangles that are originally close to one another on the template mesh. Pairs of distant triangles can also penetrate each other, but only when the mesh has undergone sufficient deformation. The observation made by SSCC suggests the use of mesh decompositions as described in 3.1.

It is worth noting that both works (Barbić and James 2010; Teng, Otaduy, and Kim 2014) use learned linear subspaces to accelerate collision detection and culling. However, since the expressivity of linear subspaces is rather limited, SSCC can only model deformations that are near the neutral pose and cannot represent larger deformations. (Teng, Otaduy, and Kim 2014) can represent large deformations, but their method assumes that a domain decomposition is manually given. Our work unifies and extends these ideas into a collision prediction algorithm that works for large deformations and does not require any additional labels other than deformed meshes.

4 LCollision: Overall Learning Algorithm

The overall learning architecture of our method is illustrated in Figure 1. Our method augments a normal mesh embedding autoencoder with an additional component to classify

the collision status. Given a latent code \mathcal{Z}_{all} defined as:

$$\mathcal{Z}_{all} = (\mathcal{Z}_0^T, \mathcal{Z}_1^T, \dots, \mathcal{Z}_{|\mathcal{Z}_0|+1}^T)^T,$$

we output a collision probability $MLP_{classifier}$ to predict whether the model generated by the decoder using \mathcal{Z}_{all} has any (self-)collision or not. We assume that the 0.5 sub-level set of $MLP_{classifier}$ corresponds to the collision-free set so that many constraints of the form $PD_{i,j} = 0$ can be replaced by a single constraint $MLP_{classifier} < 0.5$, which reduces the computational cost.

4.1 Collision Detection Architecture

In this subsection, we illustrate how we cope with the locality of self-collisions mentioned in Section 3.3 to design some parts of collision detection architecture shown as the gray ones of Figure 1, including collision state encoder and collision predictor.

Naive Subdivision: Our level-2 autoencoders inherently decompose the mesh into $|\mathcal{Z}_0|$ sub-domains. Therefore, if collisions occur within the k th sub-domain, then collisions should be inferred from \mathcal{Z}_k alone, and we use a collision predictor (CP) in the form of a multilayer perceptron (MLP) to map \mathcal{Z}_k to some collision indicator. If a pair of triangles belongs to two sub-domains, e.g., \mathcal{Z}_k and $\mathcal{Z}_{k'}$, then a possible solution is to use another MLP that takes both $(\mathcal{Z}_k^T, \mathcal{Z}_{k'}^T)^T$. However, this approach has two potential drawbacks. First, this solution requires $\mathcal{O}(|\mathcal{Z}_0|^2)$ CPs with an excessively large number of weights. Second, the latent codes of level-2 autoencoders only represent the relative residual $\mathcal{X}_0 - \bar{\mathcal{X}}_0$, while the absolute information \mathcal{X}_0 is lost.

Our Method: To avoid issues with naive subdivision, we propose using a collision state encoder (CSE) that encodes both relative and absolute information over all mesh sub-domains. CSE is an MLP that takes \mathcal{Z}_{all} and brings \mathcal{Z}_{all} through three latent layers with (512, 256, 256) neurons and ReLU activation. Finally, CSE outputs a latent code referred to as the global collision state, or $\mathcal{S}_0 = \text{CSE}(\mathcal{Z}_{all})$ for short. \mathcal{S}_0 along with \mathcal{Z}_k are then fed into a CP to obtain the collision indicator related to the k th sub-domain, i.e. collisions between pairs of triangles where at least one of the triangles belongs to the k th sub-domain. There are altogether $|\mathcal{Z}_0|$ CPs, where the k th CP maps $(\mathcal{S}_0^T, \mathcal{Z}_k^T)^T$ through four latent layers with (512, 256, 256, 128) neurons and ReLU activation. Finally, CP outputs a scalar collision indicator \mathcal{S}_k , i.e. $\mathcal{S}_k = \text{CP}(\mathcal{S}_0, \mathcal{Z}_k)$.

4.2 Collision Predictor Based on Penetration

A key issue is formulating collision indicators \mathcal{S}_k and labeling the mesh with groundtruth \mathcal{S}_i for deformed mesh data. In our application, the network output is used in optimization, and we need to give the optimizer a sense of the gradient directions. Thus, \mathcal{S}_k should not only be a collision indicator but also a collision violation metric. In other words, if $\mathcal{S}'_k > \mathcal{S}_k \geq 0$, then we must have \mathcal{S}'_k correspond to a mesh with more collisions than \mathcal{S}_k . Therefore, we use the notion of penetration depth. Given a mesh \mathcal{G} , we use the FCL library (Pan, Chitta, and Manocha 2012) to compute the squared penetration depth $PD_{p,q}^2$ of each colliding triangle pair. This

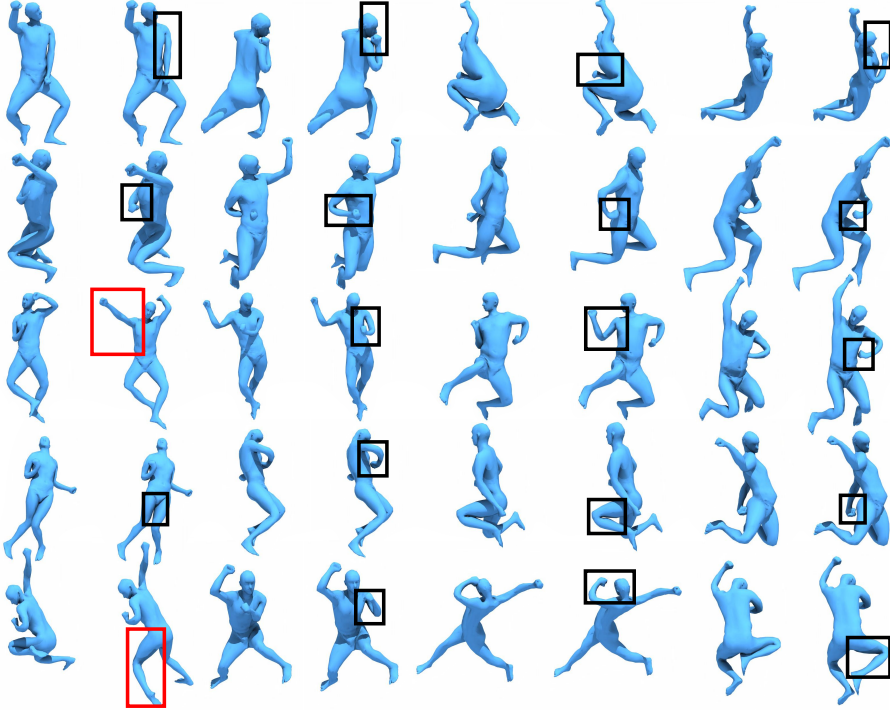


Figure 3: We illustrate 20 representative results of collision responses, where the poses on the left are the original poses directly generated using (Tan et al. 2018b), and the poses on the right are the ones after collision responses. We highlight the adjusted body parts using black boxes. In all the examples, our method can successfully avoid penetrations. However, in two cases (red boxes), our adjusted poses drift severely from the original poses.

colliding pair correlates 6 vertices in \mathcal{V} and we add $\text{PD}_{p,q}^2/6$ to each vertex as the vertex-wise collision violation. After processing all colliding triangle pairs, we have a penetration depth energy vector $\text{PDe} \in \mathbb{R}^{|\mathcal{V}|}$. The overall computation is described by Algorithm 1.

Algorithm 1 Generating Penetration Energy Vector PDe

```

1: Init  $\text{PDe} = \vec{0} \in \mathbb{R}^{|\mathcal{V}|}$ 
2: Run FCL finding the set of all collided disjoint triangle pairs
   as  $\hat{T}$ 
3: for  $(\mathbf{t}_p, \mathbf{t}_q) \in \hat{T}$  and the corresponding  $\text{PD}_{p,q}$  do
4:   for Vertex  $i$  belongs to  $\mathbf{t}_p$  and  $\mathbf{t}_q$  do
5:      $\text{PDe}_i += \frac{\text{PD}_{p,q}^2}{6}$ 
6:   end for
7: end for

```

After computing the PDe, we use the following domain-decomposed data loss to train \mathcal{S}_i :

$$\mathcal{L}_{PD} = \sum_{k=1}^{|\mathcal{Z}_0|} \|\mathcal{S}_k - \sum_{i=1}^{|\mathcal{V}|} \mathcal{M}^{ki} \text{PDe}_i\|^2 + \|\mathcal{S}_{sum} - \text{PDe-sum}\|,$$

where $\text{PDe-sum} = \sum_{i=1}^{|\mathcal{V}|} \text{PDe}_i$ is the ground truth total penetration energy and $\mathcal{S}_{sum} = \sum_{k=1}^{|\mathcal{Z}_0|} \mathcal{S}_k$ is the neural network prediction. Here, we use the same attention mask \mathcal{M}^{ki} defined in Section 3.1 to decompose the collision energy into body parts. Note that we do not have any loss terms related to \mathcal{S}_0 . However, a neural network is known to suffer from over-fitting when learning exact distance functions (Hoffer and Ailon 2015; Burges et al. 2005), including those corre-

sponding to PD. We avoid over-fitting by using the marginal ranking loss. Given two meshes, \mathcal{G} and $\hat{\mathcal{G}}$ (with approximated total penetration energy denoted as \mathcal{S}_{sum} and $\widehat{\mathcal{S}_{sum}}$) randomly sampled from the dataset, if $\hat{\mathcal{G}}$ has a higher collision violation than \mathcal{G} in terms of the total penetration energy, then we define:

$$\mathcal{L}_{rank} = \max(0, \alpha - (\widehat{\mathcal{S}_{sum}} - \mathcal{S}_{sum})),$$

and vice versa. Here, α is used as a margin to enforce ranking strictness. We choose α as the mean energy difference of the given dataset.

With the above training technique, we can predict $\mathcal{S}_1, \mathcal{S}_{|Z_0|}$ and use them as hard constraints by letting $\mathcal{S}_i = 0$, resulting in $|Z_0|$ constraints. We can further reduce the online computational cost by reducing the number of constraints to only one. To perform this computation, we train a single classifier $\text{MLP}_{classifier}(\mathcal{S}_1, \dots, \mathcal{S}_{|Z_0|})$ to summarize the information and predict whether there are any collisions throughout the human body, i.e. $\text{MLP}_{classifier}$ is an indicator of whether $\mathcal{S}_{sum} = 0$. To make sure that the 0.5 sub-level set is the collision-free subset, we use the cross entropy loss:

$$\begin{aligned} \mathcal{L}_{entropy} = & -\mathbb{I}(\text{PDe-sum} > 0) \log(\text{MLP}_{classifier}) \\ & -\mathbb{I}(\text{PDe-sum} = 0) \log(1 - \text{MLP}_{classifier}). \end{aligned}$$

4.3 Solving Constrained Optimization

Our collision response solver takes a constrained optimization in the following form:

$$\begin{aligned} \operatorname{argmin}_{\mathcal{Z}_{all}} & \| \mathcal{Z}_{all} - \mathcal{Z}_{all}^* \|^2 \\ \text{s.t. } & \text{MLP}_{classifier}(\mathcal{S}_1, \dots, \mathcal{S}_{|\mathcal{Z}_0|+1}) \leq 0.5. \end{aligned} \quad (1)$$

The idea is to provide a desired pose \mathcal{Z}_{all}^* for the bilevel decoder, and Equation 1 solves for a new \mathcal{Z}_{all} that is as close to \mathcal{Z}_{all}^* as possible and is collision-free. We solve Equation 1 using the augmented Lagrangian method implemented in LOQO (Vanderbei 1999), with all the gradient information computed via back-propagation through the neural network. This augmented Lagrangian method can start from an infeasible domain, which means that LOQO allows the hard constraints to be temporarily violated between the iterations. As a result, LOQO uses gradient information to pull the solution back to the feasible sub-manifold.

5 Evaluation

We implement our method using PyTorch (Paszke et al. 2017). All the training and testing are performed on a single desktop machine with a 32-core CPU, 32GB memory, and an NVIDIA GTX 1080Ti GPU. The training is decomposed into two stages. During the first stage, we train the two-level human pose embedding architecture using a set of N meshes. This training would optimize only the $|\mathcal{Z}_0|+1$ autoencoders and the attention mechanics. After this first stage, we could generate a much larger dataset of $M \gg N$ meshes by sampling the latent code \mathcal{Z}_{all} uniformly in the range:

$$[1.2\min(\mathcal{Z}_{all}), 1.2\max(\mathcal{Z}_{all})]^{|\mathcal{Z}_{all}|},$$

where $\min(\mathcal{Z}_{all}) < 0$, $\max(\mathcal{Z}_{all}) > 0$, and \min , \max are elementwise over all mesh samples.

We train our collision predictor and classifier on the augmented dataset while fixing the $|\mathcal{Z}_0| + 1$ autoencoders and the attention mechanics. This stage uses the loss:

$\mathcal{L} = w_{PD}\mathcal{L}_{PD} + w_{rank}\mathcal{L}_{rank} + w_{entropy}\mathcal{L}_{entropy}$, which is configured with $w_{PD} = 5$, $w_{rank} = 2$, and $w_{entropy} = 2$ and trained using a learning rate of 0.001 and a batch size of 32 over 30 epochs. We evaluate our method on three datasets: the SCAPE dataset (Anguelov et al. 2005) with $N = 71$ meshes, the MIT-Swing dataset (Vlasic et al. 2008) with $N = 150$ meshes, and the MIT Jumping dataset (Vlasic et al. 2008) with $N = 150$ meshes. For each dataset, we use all the meshes to train the embedding space during the first stage. However, during the second stage, we use $0.7M$ samples of the augmented dataset for training and $0.3M$ samples for validation. We use two settings, one with $M = 5 \times 10^4$ and the other with $M = 2.5 \times 10^6$.

Accuracy of Collision Prediction: We consider several baselines that are essentially simplified variants of our pipeline in Figure 1. We notice that the constrained optimization Equation 1 only needs the output of $\text{MLP}_{classifier}$ to be correct, which is the goal $\mathcal{L}_{entropy}$. Therefore, we consider retaining only $\mathcal{L}_{entropy}$ while removing \mathcal{L}_{rank} and \mathcal{L}_{PD} , leading to three baselines: $\mathcal{L}_{entropy} + \mathcal{L}_{PD}$, $\mathcal{L}_{entropy} + \mathcal{L}_{rank}$, and $\mathcal{L}_{entropy}$, where we use the same weights for the

Baseline	MSE	RANK	CLASSIFY
Ours	6.72×10^{-4}	6.5×10^{-3}	82.8%
$\mathcal{L}_{entropy} + \mathcal{L}_{PD}$	5.06×10^{-4}	9.4×10^{-3}	81.1%
$\mathcal{L}_{entropy} + \mathcal{L}_{rank}$	-	4.7×10^{-3}	80.7%
$\mathcal{L}_{entropy}$	-	-	80.4%
ND	6.9×10^{-4}	6.7×10^{-3}	80.2%

Table 1: We compare our method (Ours) with 4 baselines: $\mathcal{L}_{entropy} + \mathcal{L}_{PD}$, $\mathcal{L}_{entropy} + \mathcal{L}_{rank}$, $\mathcal{L}_{entropy}$, and ND (no collision decomposition). For each method, we train on the smaller dataset with $M = 5 \times 10^4$ meshes. For each trained dataset, we compare their accuracy in terms of predicting penetration depth energies (MSE), ranking penetration depth energies (RANK), and classifying collision-free meshes (CLASSIFY). Compared with $\mathcal{L}_{entropy} + \mathcal{L}_{PD}$, $\mathcal{L}_{entropy} + \mathcal{L}_{rank}$, and $\mathcal{L}_{entropy}$, we see the power of our hybrid loss to improve the overall accuracy of collision predictions. The improvement from ND to our method demonstrates that the penetration decomposition is meaningful in our framework.

retained terms. In order to demonstrate the power of collision decomposition, we compare our LCollision method with a simplified network architecture, which does not decompose the collision info into different domains. For this baseline, we simply use S_0 to predict total penetration energy \mathcal{S}_{sum} and classify collision status, and we modify \mathcal{L}_{PD} to only have $\|\mathcal{S}_{sum} - PDe-sum\|$. The other two losses \mathcal{L}_{PD} and $\mathcal{L}_{entropy}$ remain the same. This baseline is denoted as ND (no decomposition).

In Table 1, we compare the accuracy of baselines in terms of predicting penetration depth energies, ranking penetration depth energies, and classifying collision-free meshes. To ensure that our predicted penetration depth energies are accurate, we use the mean squared error (MSE) of total penetration depth energy averaged over the $0.3M$ test meshes. To ensure the accuracy of the ranking penetration depth energies, we randomly formulate a pair for each sample in the $0.3M$ test meshes, and we record the average ranking margin (RANK). To classify collision-free meshes, we use the rate of success (CLASSIFY) over the $0.3M$ test meshes.

From this ablation study, we compare ND and our method to find that penetration decomposition can improve the accuracy of collision predictions. Using penetration depth energy in the system not only gives gradient information for optimization but can also boost performance through \mathcal{L}_{PD} . \mathcal{L}_{rank} does help improve performance, but its effect is relatively minor compared to \mathcal{L}_{PD} .

M	Dataset	MSE	RANK	CLASSIFY
5×10^4	SCAPE	6.72×10^{-4}	6.5×10^{-3}	82.8%
	Swing	7.27×10^{-4}	3.38×10^{-3}	91.2%
	Jumping	6.74×10^{-4}	5.29×10^{-3}	91.6%
	SCAPE	7.80×10^{-4}	2.60×10^{-3}	94.1%
2.5×10^6	Swing	2.57×10^{-4}	2.34×10^{-3}	96.2%
	Jumping	6.34×10^{-4}	5.43×10^{-3}	95.4%

Table 2: We study the robustness of our method in terms of dataset sizes. Increasing the dataset size M can significantly boost the collision detection accuracy (CLASSIFY). This result implies that learning to predict collisions is challenging, and a larger training dataset can help improve the overall results.

Our second study inspects the robustness of our network architecture in terms of the size of the dataset. As shown in Table 2, we tested our method trained using two different M . Increasing M from 5×10^4 to 2.5×10^6 can significantly

Dataset	Time for Pan et al.	Time for ours	Speedup
SCAPE	1min 23s	1.02s	81x
Swing	5min 12s	0.91s	342x
Jumping	5min 19s	1.13s	282x

Table 3: We show the collision detection running time for our method compared with one exact collision detection algorithm (Pan, Chitta, and Manocha 2012). All datasets have 1.5×10^4 samples. Swing and Jumping have more points than SCAPE (9971 and 10002 vs 2261), and the complexity of (Pan, Chitta, and Manocha 2012) depends on the number of points, thus we spent more time on them for exact collision checking. While, they all share the same level of latent space size with SCAPE and the running times for our method are similar.

boost the collision detection accuracy (CLASSIFY). This result implies that learning to predict collisions is challenging, and a larger training dataset can help improve the overall results.

Speedup Compared with Exact Collision Checking:

The goal of our method is to speed up the collision detection process over prior exact collision and penetration methods that are applied to mesh-based representations. We compare the running time with (Pan, Chitta, and Manocha 2012) on the test set of 5×10^4 samples (1.5×10^4 samples) for the SCAPE, Swing, and Jumping datasets. To achieve the best performance for (Pan, Chitta, and Manocha 2012), we run their method using 15 threads in parallel and stop when one collision occurs or the process is reported collision-free. For our method, we feed the network with 500 models at the same time. We optimize the hyper-parameters to obtain optimal performance. We show the results in Table 3. We observe a large speedup compared to exact surface-based collision and penetration depth computation algorithms.

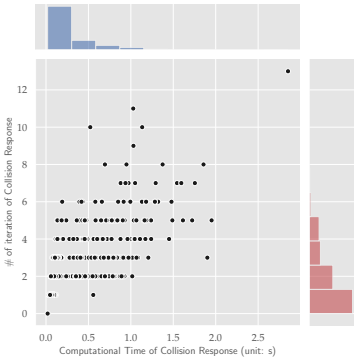


Figure 4: The joint histogram plot of the number of iterations (Y-axis) and computational time (X-axis) used for solving Equation 1 for the Swing dataset. The average # of iterations is 5.44 and the average time is 1.29s.

The Collision Response Solver: In Figure 3, we show 20 results with successful collision responses for the SCAPE dataset (more results on the other datasets given in the appendix). To profile the collision response solver quantitatively, we sample a set of 3000 random human poses by randomizing \mathcal{Z}_{all} for both the SCAPE and Swing datasets. Some of the models have self-collisions and are classified

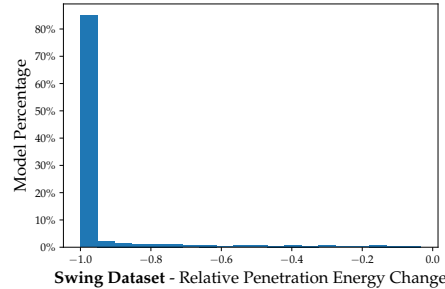


Figure 5: The histogram plot of the relative penetration depth energy change for successful examples, after solving Equation 1 for the Swing dataset. We see results with decreased penetration energy as successful ones. Our method achieves a success rate of 85.1%, and we observed an average relative decrease of 94.3% for these models compared to original penetration energy.

correctly by our learning-based collision detection algorithm. For each of these meshes, we solve Equation 1, and the solution will be one of two cases: either the solution will have decreased penetration energy or it is a hard case that our optimization method fails to solve. We consider a collision response solve successful in the first case. On the SCAPE dataset, our method achieves a success rate of 85.6%, and we observe a relative decrease of 80.9% for these models compared to the original penetration depth energy. On the Swing dataset, our method achieves a success rate of 85.1% and we observe a relative decrease of 94.3% for these models. In Figure 4, we plot the number of iterations and computational time used by the constrained optimizer until convergence for the Swing dataset. The average iteration is 5.44 and the average time is 1.29s. For the SCAPE dataset, the average iteration is 2.09 and the average time is 0.25s. In Figure 5, we highlight the distribution of relative penetration energy change for successful collision response models.

6 Conclusion, Limitations, and Future Work

We present a method for learning the collision-free human pose sub-manifold. We use a mesh embedding autoencoder to learn a full human pose manifold and augment it with an additional component to classify the collision and other hard constraints. Our method decomposes the mesh into several sub-domains and learns the decision boundary of the collision-free sub-manifold by reusing the decomposed sub-domains. Specifically, we learn to predict the penetration depths aggregated to each sub-domain and then use a binary classifier to predict whether a given mesh has any collisions. When evaluated on the SCAPE dataset, our method achieves a success rate of 94.1% in predicting collisions and a success rate of 85.6% in collision responses. To the best of our knowledge, ours is the first approach that can obtain high accuracy in terms of handling non-penetration constraints in a learning framework.

Our method has some limitations. Being a learning-based method, our collision predictor cannot achieve a 100% success rate, in contrast to analytic methods (Barbić and James 2010). This could pose a problem when our method is used to generate computer animations, where a few missed collisions can have a considerable impact on the overall simulation accuracy. In the future, we would like to consider active

learning to collect more data and improve the accuracy of the collision predictor in a self-supervised manner, as shown in (Pan, Zhang, and Manocha 2013) for rigid objects. A second issue is the use of a continuous constraint optimizer (Vanderbei 1999) for collision responses. These solvers require twice-differentiable hard constraints, which is not the case in our application because we use non-differentiable ReLU activation units. It is worth exploring new constraint optimization solvers that could work with non-smooth constraints specified by a neural network. Finally, our method sheds light on new approaches that could incorporate hard constraints into a neural network. We plan to extend our work by considering other types of hard constraints such as dynamics and accurate collision response models.

References

- Agarwal, A.; and Triggs, B. 2005. Recovering 3D human pose from monocular images. *IEEE transactions on pattern analysis and machine intelligence* 28(1): 44–58.
- Agrawal, A.; Amos, B.; Barratt, S.; Boyd, S.; Diamond, S.; and Kolter, J. Z. 2019. Differentiable convex optimization layers. In *Advances in Neural Information Processing Systems*, 9558–9570.
- Anguelov, D.; Srinivasan, P.; Koller, D.; Thrun, S.; Rodgers, J.; and Davis, J. 2005. SCAPE: shape completion and animation of people. In *ACM SIGGRAPH*, 408–416.
- Bagautdinov, T.; Wu, C.; Saragih, J.; Fua, P.; and Sheikh, Y. 2018. Modeling facial geometry using compositional vaes. In *Proceedings of the IEEE Conference on Computer Vision and Pattern Recognition*, 3877–3886.
- Barbić, J.; and James, D. L. 2010. Subspace Self-Collision Culling. *ACM Trans. on Graphics (SIGGRAPH 2010)* 29(4): 81:1–81:9.
- Boggs, P. T.; and Tolle, J. W. 1995. Sequential quadratic programming. *Acta numerica* 4: 1–51.
- Bouritsas, G.; Bokhnyak, S.; Ploumpis, S.; Bronstein, M.; and Zafeiriou, S. 2019. Neural 3d morphable models: Spiral convolutional networks for 3d shape representation learning and generation. In *Proceedings of the IEEE International Conference on Computer Vision*, 7213–7222.
- Bridson, R.; Fedkiw, R.; and Anderson, J. 2002. Robust treatment of collisions, contact and friction for cloth animation. In *Proceedings of the 29th annual conference on Computer graphics and interactive techniques*, 594–603.
- Burgard, W.; Brock, O.; and Stachniss, C. 2008. *A Fast and Practical Algorithm for Generalized Penetration Depth Computation*, 265–272.
- Burges, C.; Shaked, T.; Renshaw, E.; Lazier, A.; Deeds, M.; Hamilton, N.; and Hullender, G. 2005. Learning to rank using gradient descent. In *Proceedings of the 22nd international conference on Machine learning*, 89–96.
- Gao, L.; Lai, Y.-K.; Yang, J.; Ling-Xiao, Z.; Xia, S.; and Kobbelt, L. 2019. Sparse data driven mesh deformation. *IEEE transactions on visualization and computer graphics* .
- Hanocka, R.; Hertz, A.; Fish, N.; Giryes, R.; Fleishman, S.; and Cohen-Or, D. 2019. MeshCNN: A network with an edge. *ACM Transactions on Graphics* 38(4): 90. ISSN 15577368. doi:10.1145/3306346.3322959.
- Hoffer, E.; and Ailon, N. 2015. Deep metric learning using triplet network. In *International Workshop on Similarity-Based Pattern Recognition*, 84–92. Springer.
- Kervadec, H.; Dolz, J.; Tang, M.; Granger, E.; Boykov, Y.; and Ayed, I. B. 2019. Constrained-CNN losses for weakly supervised segmentation. *Medical image analysis* 54: 88–99.
- Kim, Y.; Lin, M.; and Manocha, D. 2018. Collision and proximity queries. *Handbook of Discrete and Computational Geometry* .
- Kim, Y. J.; Otaduy, M. A.; Lin, M. C.; and Manocha, D. 2002. Fast penetration depth computation for physically-based animation. In *Proceedings of the 2002 ACM SIGGRAPH/Eurographics symposium on Computer animation*, 23–31.
- Leibe, B.; Seemann, E.; and Schiele, B. 2005. Pedestrian detection in crowded scenes. In *2005 IEEE Computer Society Conference on Computer Vision and Pattern Recognition (CVPR’05)*, volume 1, 878–885. IEEE.
- Li, Y.; Wu, J.; Tedrake, R.; Tenenbaum, J. B.; and Torralba, A. 2019. Learning Particle Dynamics for Manipulating Rigid Bodies, Deformable Objects, and Fluids. In *ICLR*.
- Marquez Neila, P.; Salzmann, M.; and Fua, P. 2017. Imposing Hard Constraints on Deep Networks: Promises and Limitations URL <http://infoscience.epfl.ch/record/262884>.
- Nandwani, Y.; Pathak, A.; Singla, P.; et al. 2019. A Primal Dual Formulation For Deep Learning With Constraints. In *Advances in Neural Information Processing Systems*, 12157–12168.
- Pan, J.; Chitta, S.; and Manocha, D. 2012. FCL: A general purpose library for collision and proximity queries. In *2012 IEEE International Conference on Robotics and Automation*, 3859–3866. IEEE.
- Pan, J.; Zhang, X.; and Manocha, D. 2013. Efficient penetration depth approximation using active learning. *ACM Transactions on Graphics (TOG)* 32(6): 1–12.
- Paszke, A.; Gross, S.; Chintala, S.; Chanan, G.; Yang, E.; DeVito, Z.; Lin, Z.; Desmaison, A.; Antiga, L.; and Lerer, A. 2017. Automatic differentiation in pytorch.
- Pham, T.; De Magistris, G.; and Tachibana, R. 2018. OptLayer - Practical Constrained Optimization for Deep Reinforcement Learning in the Real World. In *2018 IEEE International Conference on Robotics and Automation (ICRA)*, 6236–6243.
- Qi, C. R.; Su, H.; Mo, K.; and Guibas, L. J. 2017. Pointnet: Deep learning on point sets for 3d classification and segmentation. In *Proceedings of the IEEE conference on computer vision and pattern recognition*, 652–660.
- Qiao, Y.-L.; Liang, J.; Koltun, V.; and Lin, M. C. 2020. Scalable Differentiable Physics for Learning and Control. *arXiv preprint arXiv:2007.02168* .

- Ranjan, A.; Bolkart, T.; Sanyal, S.; and Black, M. J. 2018. Generating 3D faces using convolutional mesh autoencoders. In *Proceedings of the European Conference on Computer Vision (ECCV)*, 704–720.
- Ravi, S. N.; Dinh, T.; Lokhande, V. S.; and Singh, V. 2019. Explicitly imposing constraints in deep networks via conditional gradients gives improved generalization and faster convergence. In *Proceedings of the AAAI Conference on Artificial Intelligence*, volume 33, 4772–4779.
- Rogez, G.; Rihan, J.; Ramalingam, S.; Orrite, C.; and Torr, P. H. 2008. Randomized trees for human pose detection. In *2008 IEEE Conference on Computer Vision and Pattern Recognition*, 1–8. IEEE.
- Shi, X.; Zhou, K.; Tong, Y.; Desbrun, M.; Bao, H.; and Guo, B. 2007. Mesh puppetry: cascading optimization of mesh deformation with inverse kinematics. In *ACM SIGGRAPH 2007 papers*, 81–es.
- Smith, B.; Goes, F. D.; and Kim, T. 2018. Stable neo-hookean flesh simulation. *ACM Transactions on Graphics (TOG)* 37(2): 1–15.
- Tan, Q.; Gao, L.; Lai, Y.-K.; and Xia, S. 2018a. Variational autoencoders for deforming 3d mesh models. In *Proceedings of the IEEE conference on computer vision and pattern recognition*, 5841–5850.
- Tan, Q.; Gao, L.; Lai, Y.-K.; Yang, J.; and Xia, S. 2018b. Mesh-based autoencoders for localized deformation component analysis. In *Thirty-Second AAAI Conference on Artificial Intelligence*.
- Tang, M.; Curtis, S.; Yoon, S.-E.; and Manocha, D. 2009. ICCD: Interactive continuous collision detection between deformable models using connectivity-based culling. *IEEE Transactions on Visualization and Computer Graphics* 15(4): 544–557.
- Teng, Y.; Otaduy, M. A.; and Kim, T. 2014. Simulating Articulated Subspace Self-Contact. *ACM Trans. Graph.* 33(4). ISSN 0730-0301. doi:10.1145/2601097.2601181. URL <https://doi.org/10.1145/2601097.2601181>.
- Toshev, A.; and Szegedy, C. 2014. Deeppose: Human pose estimation via deep neural networks. In *Proceedings of the IEEE conference on computer vision and pattern recognition*, 1653–1660.
- Tretschk, E.; Tewari, A.; Zollhöfer, M.; Golyanik, V.; and Theobalt, C. 2020. DEMEA: Deep Mesh Autoencoders for Non-Rigidly Deforming Objects. *European Conference on Computer Vision (ECCV)*.
- Vanderbei, R. J. 1999. LOQO user’s manual—version 3.10. *Optimization methods and software* 11(1-4): 485–514.
- Villegas, R.; Yang, J.; Ceylan, D.; and Lee, H. 2018. Neural kinematic networks for unsupervised motion retargetting. In *Proceedings of the IEEE Conference on Computer Vision and Pattern Recognition*, 8639–8648.
- Vlasic, D.; Baran, I.; Matusik, W.; and Popović, J. 2008. Articulated mesh animation from multi-view silhouettes. In *ACM SIGGRAPH 2008 papers*, 1–9.
- Wang, P.-S.; Liu, Y.; and Tong, X. 2020. Deep Octree-based CNNs with Output-Guided Skip Connections for 3D Shape and Scene Completion.
- Zhang, L.; Kim, Y. J.; Varadhan, G.; and Manocha, D. 2007. Generalized penetration depth computation. *Computer-Aided Design* 39(8): 625–638.